1-1-2014

Rapid synthesis of Li4Ti5O12/graphene composite with superior rate capability by a microwave-assisted hydrothermal method

Yi Shi
University of Wollongong, ys551@uowmail.edu.au

Jie Gao
Cornell University

Hector D. Abruna
Cornell University

Hua-Kun Liu
University of Wollongong, hua@uow.edu.au

Huijun Li
University of Wollongong, huijun@uow.edu.au

See next page for additional authors

Rapid synthesis of Li4Ti5O12/graphene composite with superior rate capability by a microwave-assisted hydrothermal method

Abstract

Li4Ti5O12 microspheres composed of nanoflakes wrapped in graphene nanosheets have been synthesized by an advanced microwave-hydrothermal (MW-HT) method for the preparation following by an annealing step. Microwave-assisted synthesis processes are appealing, as they can rapidly synthesize materials with a high degree of control of particle size and morphology at low cost. The resultant composite reveals a unique loose structure which could avoid the restacking of graphene sheets and offer rapid lithium ion diffusion paths. Therefore the Li4Ti5O12/graphene electrode has highly desirable properties: a specific capacity approaching the theoretical value, stable cycling, and exceptional rate capability. The composite also can be a good indicator of the remained charge and discharge capacity since it presents a curved charge and discharge line instead of a stable plateau.

Keywords

rapid, synthesis, li4ti5o12, graphene, composite, superior, rate, capability, hydrothermal, microwave, method, assisted

Disciplines

Engineering | Physical Sciences and Mathematics

Publication Details

Shi, Y., Gao, J., Abruna, H. D., Liu, H., Li, H., Wang, J. & Wu, Y. (2014). Rapid synthesis of Li4Ti5O12/graphene composite with superior rate capability by a microwave-assisted hydrothermal method. Nano Energy, 8 297-304.

Authors

Yi Shi, Jie Gao, Hector D. Abruna, Hua-Kun Liu, Huijun Li, Jiazhao Wang, and Yuping Wu

Rapid microwave-assisted hydrothermal synthesis of $Li_4Ti_5O_{12}$/graphene composite with superior rate capability

Yi Shi

Introduction:

Recently, there has been a great interest in developing rechargeable lithium ion batteries (LIBs) for applications in automobiles and stationary power storage[1, 2] to address increasing global energy consumption as well as the critical issue of climate change. [3, 4] Although LIBs have gained commercial success and conquered the portable market, their implementation in electric transportation keeps being postponed due to low power, high cost, and safety issues.[5, 6] The commercial anode material, graphite, has a small lithium diffusion coefficient and experiences large volume variation of 9% during the lithium intercalation/de-intercalation process. In addition, it has severe safety issues of dendritic lithium growth, due to its low potential (only about 0.2 V versus Li^+/Li). Especially at high rates, polarization would considerably lower its potential further, causing the birth of lithium dendrites and the consequent safety issues. Furthermore, the thick solid electrolyte interphase (SEI) layer on its surface could also introduce kinetic problems for fast charge and discharge. [7]Among the various anode materials for LIBs, spinel lithium titanate ($Li_4Ti_5O_{12}$) is considered an appealing candidate. $Li_4Ti_5O_{12}$ has been found to change its structure negligibly during the discharge/charge process, and possesses good lithium ion mobility and a long and stable voltage plateau, together with low cost, environmental friendliness, and enhanced safety.[7-9] In addition, as the high equilibrium potential of the Ti^{4+}/Ti^{3+} redox couple is above the reduction potential of common electrolyte solvents, an SEI film caused by solvent reduction does not form during the charge and discharge process. All of these merits make $Li_4Ti_5O_{12}$ more competitive as a safe anode material for high power LIBs. As $Li_4Ti_5O_{12}$ is an insulator, [10] however, the low electrical conductivity becomes a major drawback, which is especially unfavorable to high rate capability,[11-13] As nanosized particles can reduce the lithium-ion diffusion path, particle size reduction or special nanostructural design is effective in improving its rate capability,[14, 15], a particular concern because the polarization of the electrode becomes serious when charged/discharged at a higher current density. Until now, various wet-chemical methods have been developed and used for the production of pure-phase nanosized $Li_4Ti_5O_{12}$ particles, but agglomeration is usually inevitable during drying. Substituting an aliovalent metal into the Ti^{4+} or Li^+ sites is another important strategy for conductivity improvement. This is expected to produce a high reversible capacity, as well as maintaining high rate performance. Various other approaches have been used, such as surface coatings with conductive material[11, 12, 16] and doping with aliovalent metal ions.[11, 17, 18]

Graphene, as a two-dimensional macromolecular sheet of carbon atoms with a honeycomb structure, has excellent electronic conductivity and mechanical properties, and may be the ideal conductive additive for hybrid nanostructured electrodes. Other advantages of graphene include high surface area (theoretical value of 2630 $m^2 g^{-1}$) for improved interfacial contact and the potential for low manufacturing costs. [19-22] The graphene wrapping process provides interconnected open pores that favor electrolyte absorption and reduce the diffusion paths of the lithium ions.[4, 23-27]

The synthesis method for materials used in commercial electric vehicles and hybrid electric vehicles (EVs and HEVs) should combine the advantages of simplicity, rapid synthesis, safety, and low cost. The hydrothermal route for synthesizing $Li_4Ti_5O_{12}$ composites (including $Li_4Ti_5O_{12}$/graphene composite) is particularly successful in terms of controlling the chemical composition, particle shape, and crystallite size in a simple and inexpensive way,[11, 28] although the conventional hydrothermal process involves a very complicated reaction route and long hydrothermal process (5–12 h) to synthesize $Li_4Ti_5O_{12}$ and produces larger submicron size particles with a wider distribution of particle size. Microwave-assisted

synthesis processes are appealing, as they can synthesize materials rapidly with a high degree of control of particle size and morphology at low cost.[29-31] Therefore, this method is more favorable for industrial manufacturing compared with the conventional hydrothermal synthesis.

This paper reports an advanced microwave-hydrothermal (MW-HT) method for the preparation of $Li_4Ti_5O_{12}$ microspheres composed of nanoflakes wrapped in graphene nanosheets. The structure, morphology, and electrochemical properties of the $Li_4Ti_5O_{12}$/graphene composite are also presented in this paper.

Experiment:

2.1 Materials synthesis

Graphene oxide (GO) was prepared according to the method reported by Hummers from graphite powder (Aldrich, powder, < 20 μm, synthetic). $Li_4Ti_5O_{12}$/graphene composite was prepared by an MW-HT synthesis process. The microwave-assisted hydrothermal procedure is adapted from a previously reported hydrothermal method.[14] For synthesizing $Li_4Ti_5O_{12}$, first, 8 mmol LiOH was dissolved in 20 mL deionized water, 1 mL 30% H_2O_2 was then added to the solution, and finally, 2 mmol titanium isopropoxide (TP) was added to the solution and stirred for 20 min. The as-prepared solution was transferred to a polytetrafluoroethylene (PTFE)-lined autoclave, which was sealed for microwave irradiation. The autoclave was put under microwave-assisted hydrothermal treatment at 150 ^oC for 15 min to yield the as-prepared lithium titanium oxide precursor. The as-prepared lithium titanium oxide precursor was collected and dissolved in 100 mL deionized water with 0.25 ml 70% hydrazine hydrate and 0.1 g GO after 2 h of ultrasonic dispersion time. After being further stirred for 30 min, the mixture was refluxed at 95 °C for 24 h. The grey powder was filtrated and washed several times with deionized water and acetone, then dried at 80 °C for 4 h in a vacuum oven, with a following sintering at 500 °C for 2 h under Ar atmosphere to yield the $Li_4Ti_5O_{12}$/graphene composite (denoted as LTO/G). As a reference, $Li_4Ti_5O_{12}$ (denoted as LTO) was also prepared following the typical microwave-hydrothermal method. First, 4 mmol LiOH was dissolved in 20 mL deionized water, and 2 mmol titanium isopropoxide (TP) was added to the solution and stirred for 20 min. The as-prepared solution was put under microwave-assisted hydrothermal treatment at 180 ^oC for 15 min followed by sintering at 700 °C for 2 h under air atmosphere.

2.2 Material characterization:

X-Ray diffraction (XRD) (GBC MMA) data was collected from powder samples at a scanning rate of 2° min^{-1} for 2θ in the range of 10–50°. Traces^{TM} software in combination with the Joint Committee on Powder Diffraction Standards (JCPDS) powder diffraction files was used to identify the phases present. Raman analysis was performed using a Raman spectrometer (Jobin Yvon HR800) employing a 10 mW helium/neon laser at 632.8 nm. The amount of graphene in the samples was estimated using a Mettler-Toledo thermogravimetric analysis/differential scanning calorimetry (TGA/DSC) 1 STARe System from 50–800 °C at 5°C min^{-1} in air flux. The morphologies of the samples were investigated by field emission scanning electron microscopy (FE-SEM; JEOL JSM-7500FA). Transmission electron microscopy (TEM) investigations were performed using a 200 kV JEOL 2011. TEM samples were prepared by deposition of ground particles onto holey carbon support films, with care taken to ensure that selected area electron diffraction (SAED) and high resolution TEM contrast were obtained only from sample regions located over holes in the holey carbon support films. To test the electrochemical performance, electrodes were prepared by pasting a mixture of the $Li_4Ti_5O_{12}$ or $Li_4Ti_5O_{12}$/graphene anode material, carbon black, and sodium carboxymethyl cellulose (CMC) in a weight ratio of 80: 10: 10 on copper foil, followed by a drying in a vacuum oven at 150 °C for 2 h. CR 2032 coin-type cells were assembled in an Ar-filled glove box (Mbraun, Unilab, Germany) using lithium metal foil as the counter electrode and 1 M $LiPF_6$ solution in ethylene carbonate/diethyl

carbonate as the electrolyte (1: 1 by volume, provided by MERCK KGaA, Germany). The cells were galvanostatically charged and discharged in the range of 1-3 V at different rates using a computer-controlled charger system manufactured by Land Battery Testers. Electrochemical impedance spectroscopy (EIS) was performed on the electrodes using a Biologic VMP3 electrochemistry workstation. The AC amplitude was 5 mV, and the frequency range applied was 100 kHz to 0.01 Hz.

Results and discussion

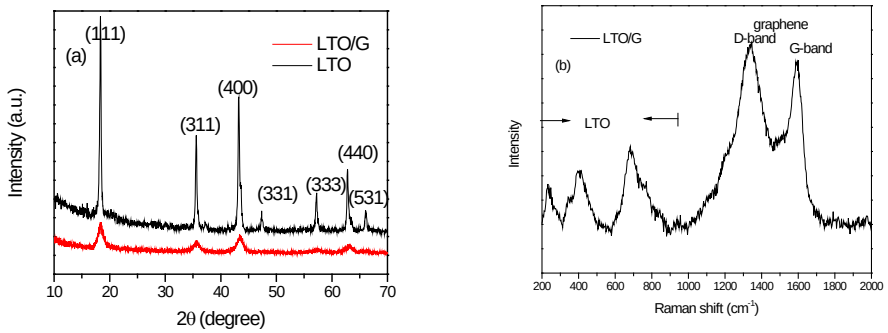

Figure 1 a) XRD patterns of $Li_4Ti_5O_{12}$ and $Li_4Ti_5O_{12}$/graphene composites, and b) Raman spectrum of $Li_4Ti_5O_{12}$/graphene composite.

Comment [HL1]: Move the corresponding text before the Figs in whole manuscript

Comment [HL2]: In Fig. 1b, the note '– LTO/G' may be changed as 'LTO/G'

Fig. 1 shows the X-ray diffraction (XRD) patterns obtained from the $Li_4Ti_5O_{12}$ and $Li_4Ti_5O_{12}$/graphene composite, in which the majority of diffraction lines can be indexed to lithium titanium oxide hydrate (orthorhombic, space group *C*, JCPDS card No. 47-0123). Diffraction peaks which might appear for graphene carbon are absent, most likely because they are below the limits of detection by XRD. The absence of a reflection peak at approximately 11^o indicates that the GO cannot be distinguished, consistent with full or partial reduction to graphene. The low intensity of the peaks of the $Li_4Ti_5O_{12}$/graphene composite may be caused by the presence of graphene during the synthesis and the low annealing temperature. The Raman spectrum of the $Li_4Ti_5O_{12}$/graphene sample shows five peaks in the range of 200-1000 cm^{-1}, which are similar to those of previously reported $Li_4Ti_5O_{12}$. The five Raman peaks are a feature of the spinel structure (A_{1g} + E_g + $3F_{2u}$). In lithium titanate, the frequencies in the 700-550 cm^{-1} region are assigned to Ti-O stretching vibrations in "TiO_6" octahedra. In oxides where lithium is located in "LiO_6" octahedra, the frequencies of the Li-O stretching vibrations are known to lie within the 250-400 cm^{-1} region, whereas in "LiO_4" tetrahedra, the frequencies of the Li-O stretches are known to lie within the 400-550 cm^{-1} range. Lithium only takes an octahedral position in $Li_4Ti_5O_{12}$, but in Li_2TiO_3, lithium occupies both octahedral and tetrahedral positions. The bands in the range of 1200-1460 cm^{-1} and 1470-1730 cm^{-1} are attributed to the D-band (K-point phonons of A_{1g} symmetry) and G-band (E_{2g} phonons of C sp^2 atoms) of graphene.[14] Therefore, the Raman spectrum [Figure 1(b)] indicates the presence of $Li_4Ti_5O_{12}$ and graphene in the composite and the absence of Li_2TiO_3.

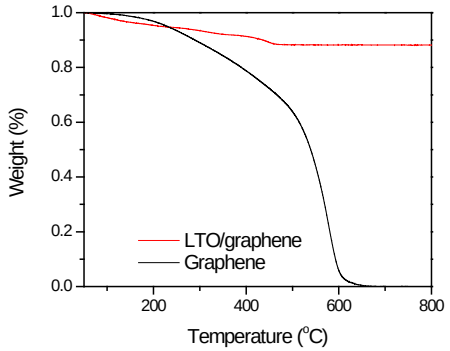

Figure 2 TGA curves of graphene and $Li_4Ti_5O_{12}$/graphene.

Comment [HL3]: Y-axis, the scale 0.0 – 1.0 may be changed to 0 – 100, Y-axis title: mass retained
Mark 11.8% for Graphene in composite

The amount of graphene in the samples was estimated using a Mettler-Toledo thermogravimetric analysis/differential scanning calorimetry (TGA/DSC) instrument (Figure 2). The results show a typical TGA curve of the $Li_4Ti_5O_{12}$/graphene composite sample along with that of a graphene sample. $Li_4Ti_5O_{12}$ remains stable during the heating, while graphene should be decomposed above 700°C, leading to a decrease in the total weight of the composite. The weight loss of the $Li_4Ti_5O_{12}$/graphene after the oxidation could be translated into the amount of graphene in the $Li_4Ti_5O_{12}$/graphene composite. By this method, the amount of graphene in the $Li_4Ti_5O_{12}$/graphene was estimated to be approximately 11.8 wt. %.

Comment [HL4]: not correct.
Graphene is burned out (to form CO2) during heating process

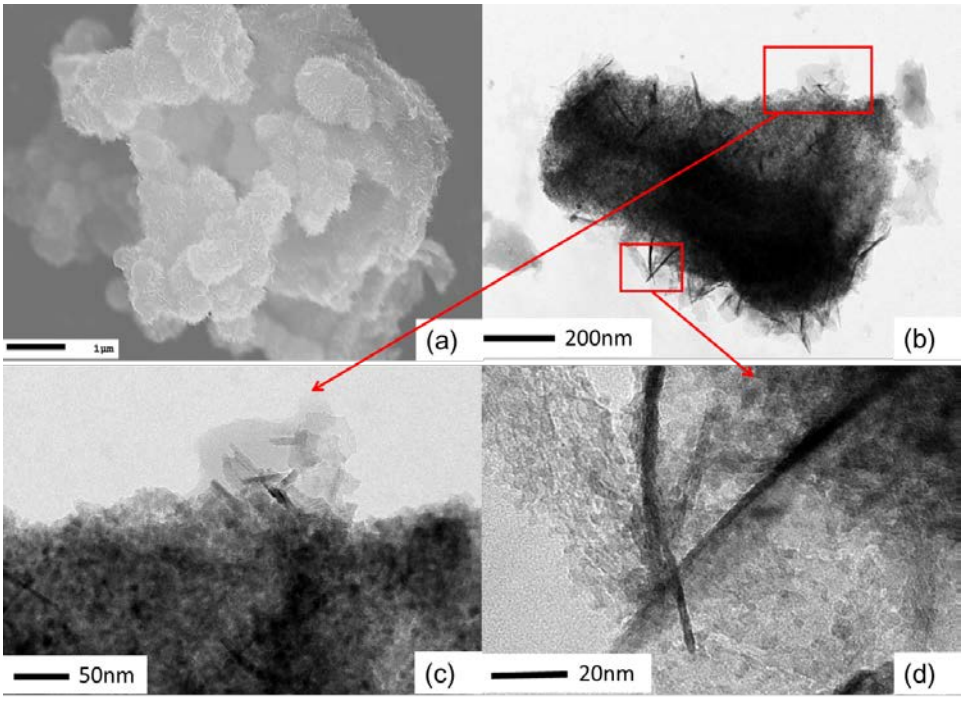

Figure 3 Electron micrographs of $Li_4Ti_5O_{12}$/graphene composite: (a) FE-SEM secondary electron micrograph of a large area of $Li_4Ti_5O_{12}$/graphene; (b) TEM micrograph of $Li_4Ti_5O_{12}$/graphene; (c) and (d) TEM micrographs of the area indicated by the rectangle marked with red lines in (b).

Comment [HL5]: Point out Graphene nanosheets or nanoflakes
What are the two long dark parts

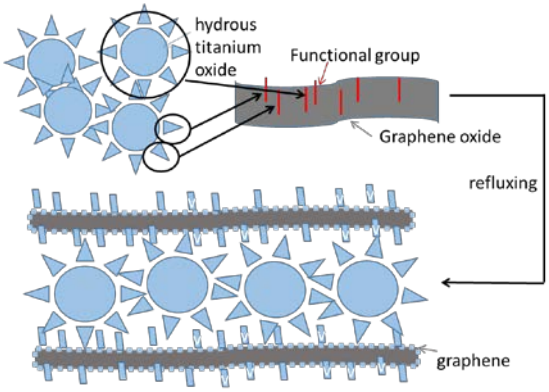

Figure 4 Schematic diagram of the formation and the structure of the $Li_4Ti_5O_{12}$ and the graphene nanosheets bridging the $Li_4Ti_5O_{12}$/graphene, which could be responsible for the superior properties of the $Li_4Ti_5O_{12}$/graphene composite.

Comment [HL6]: Need more details to describe the schematic diagram in text
Are the rectangular crystals for LTO?

Figure 3 shows FE-SEM [Fig. 3(a)] and TEM [Fig. 3(b, c, d)] images obtained from the $Li_4Ti_5O_{12}$/graphene composite. The composite exhibits a unique morphology, which includes separated flakes and also microspheres composed of nanoflakes distributed on the graphene nanosheets. The average size of the spheres is a few hundred nanometers, and the size of the graphene sheets could be several micrometers according to the FE-SEM image [Fig. 3(a)]. Fig. 3(b) displays a high resolution TEM (HRTEM) image of a single microsphere loaded on a large piece of graphene nanosheet. The high magnification images [Fig. 3(c, d)] confirm that the graphene sheets are fully covered by not only the flakes (> 100 nm in size), but also nanoparticles (around 10 nm in size). The microspheres are also composed of not only the flakes, but also the nanoparticles. The nanoparticles and flakes covering the graphene nanosheets could greatly reduce the restacking of graphene sheets and form a porous network between the $Li_4Ti_5O_{12}$ and graphene, which is believed to facilitate the penetration of the electrolyte to the surface of the active materials. Furthermore, the loose structure of the submicron-sized spheres and the small size of the nanoparticles could favour a high rate of lithium ion insertion and high efficiency of use of the graphene surface area. Therefore, in this kind of structure, the bridging graphene nanosheets can form an effective conducting network resulting in superior rate capability and enhanced reversible capacity. This unique morphology may be caused by the special *in-situ* synthesis steps and the low annealing temperature, which tend to reduce agglomeration. A schematic drawing of this morphology is shown in Figure 4.

The electrochemical performance of the $Li_4Ti_5O_{12}$ and $Li_4Ti_5O_{12}$/graphene composite is shown in Figures 5and 6.

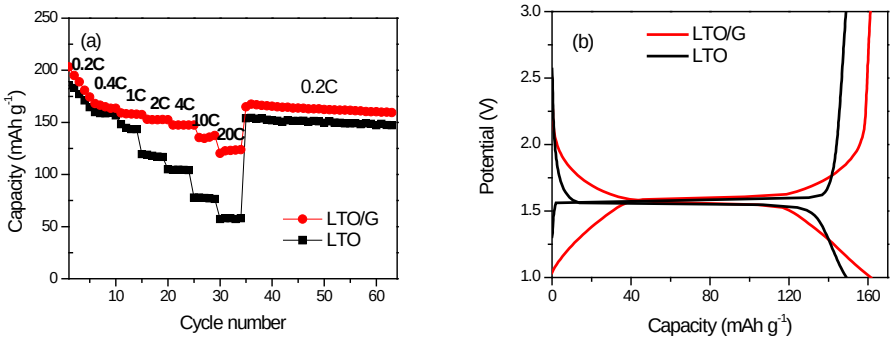

Figure 5 Electrochemical performance of the $Li_4Ti_5O_{12}$ and $Li_4Ti_5O_{12}$/graphene composite: (a) rate performance and cycling performance of the $Li_4Ti_5O_{12}$ and $Li_4Ti_5O_{12}$/graphene composite, (b) typical discharge and charge profiles at 0.2 C;

Different rates of charge-discharge were also used to investigate the electrochemical performance of the $Li_4Ti_5O_{12}$ and $Li_4Ti_5O_{12}$/graphene composite, as shown in Figure 5(a). Less than 1% capacity is lost after changing the current density from 0.2 to 20 C step by step and back to 0.2 C, showing the good stability of the $Li_4Ti_5O_{12}$ and $Li_4Ti_5O_{12}$/graphene composite electrodes. To compare the rate capability, the C rate is based only on the $Li_4Ti_5O_{12}$, and 1 C is 170 mA g^{-1}. The $Li_4Ti_5O_{12}$/graphene composite exhibits an obviously much improved performance over the $Li_4Ti_5O_{12}$ [Figure 5(a)]. It delivers a high charge capacity close to the theoretical capacity at a low current density of 0.2 C and 123 mAh g^{-1} at the high current density of 20 C, which is more than twice that of the $Li_4Ti_5O_{12}$. The gentle slope in the charge/discharge curves of the $Li_4Ti_5O_{12}$/graphene composite may be attributed to the graphene as well as the low crystallinity [Figure 5(b)]. These results are comparable to those for reported $Li_4Ti_5O_{12}$/graphene composites or even better,[11, 27, 28, 32, 33] which could be attributable to the special morphology.

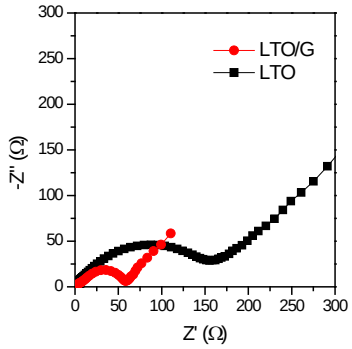

Figure 6 Nyquist plots of $Li_4Ti_5O_{12}$ and $Li_4Ti_5O_{12}$/graphene composite after 5 cycles.

The Nyquist plots (EIS spectra) show a compressed semicircle in the high to medium frequency range of each spectrum, which describes the charge transfer resistance (R_{ct}) for these electrodes, and an approximately 45° inclined line in the low-frequency range, which could be considered as Warburg impedance (Z_W), which is associated with the lithium-ion diffusion in the bulk of the active material. The high-frequency intercept of the semicircle is related to the uncompensated resistance (R_u), while the diameter of the compressed semicircle is related to the charge transfer resistance (R_{ct}). [30] After simulating the compressed semicircle for both samples, the values of R_{ct} for the $Li_4Ti_5O_{12}$ and $Li_4Ti_5O_{12}$/graphene electrodes after 5 cycles were calculated to be 158 and 61 Ω, respectively, indicating the enhanced ionic conductivity of the $Li_4Ti_5O_{12}$/graphene composite.

Conclusions

In conclusion, a highly ordered $Li_4Ti_5O_{12}$/graphene nanocomposite has been developed by a rapid, facile microwave-hydrothermal route. The resultant composite reveals a unique morphology, in which the flakes and submicron-sized spheres are loaded on graphene nanosheets. This kind of loose structure could avoid the restacking of graphene sheets and offer rapid lithium ion diffusion paths.The results clearly demonstrate that the $Li_4Ti_5O_{12}$/graphene electrode has highly desirable properties: a specific capacity approaching the theoretical value, stable cycle life, and exceptional rate capability. Therefore,

$Li_4Ti_5O_{12}$/graphene electrode is a promising candidate for the development of high-performance, low-cost, advanced lithium batteries directed to the electric and hybrid electric vehicle markets.

References

1. Tarascon, J.-M.; Armand, M. *Nature* **2001,** 414, (6861), 359-367.
2. Kang, K.; Meng, Y. S.; Breger, J.; Grey, C. P.; Ceder, G. *Science* **2006,** 311, (5763), 977-980.
3. Yu, G.; Hu, L.; Vosgueritchian, M.; Wang, H.; Xie, X.; McDonough, J. R.; Cui, X.; Cui, Y.; Bao, Z. *Nano Lett.* **2011,** 11, (7), 2905-2911.
4. Shi, Y.; Wang, J.; Chou, S.; Wexler, D.; Li, H.; Ozawa, K.; Liu, H.; Wu, Y. *Nano Lett.* **2013,** 13, (10), 4715-4720.
5. Endo, M.; Kim, C.; Nishimura, K.; Fujino, T.; Miyashita, K. *Carbon* **2000,** 38, (2), 183-197.
6. Tang, Y.; Yang, L.; Fang, S.; Qiu, Z. *Electrochim. Acta* **2009,** 54, (26), 6244-6249.
7. Kim, H.; Bak, S.; Kim, K. *Electrochem. Commun.* **2010,** 12, (12), 1768-1771.
8. Ohzuku, T.; Ueda, A.; Yamamoto, N. *J. Electrochem. Soc.* **1995,** 142, (5), 1431-1435.
9. Chen, J.; Yang, L.; Fang, S.; Hirano, S.-i.; Tachibana, K. *J. Power Sources* **2011**.
10. Harrison, M.; Edwards, P.; Goodenough, J. *Philosophical Magazine B* **1985,** 52, (3), 679-699.
11. Shen, L.; Yuan, C.; Luo, H.; Zhang, X.; Yang, S.; Lu, X. *Nanoscale* **2011,** 3, (2), 572-574.
12. Wang, G.; Gao, J.; Fu, L.; Zhao, N.; Wu, Y.; Takamura, T. *J. Power Sources* **2007,** 174, (2), 1109-1112.
13. Sha, Y.; Zhao, B.; Ran, R.; Cai, R.; Shao, Z. *Journal of Materials Chemistry A* **2013,** 1, (42), 13233-13243.
14. Chou, S.-L.; Wang, J.-Z.; Liu, H.-K.; Dou, S.-X. *J. Phys. Chem. C* **2011,** 115, (32), 16220-16227.
15. Lee, S. C.; Lee, S. M.; Lee, J. W.; Lee, J. B.; Lee, S. M.; Han, S. S.; Lee, H. C.; Kim, H. J. *J. Phys. Chem. C* **2009,** 113, (42), 18420-18423.
16. Prakash, A.; Manikandan, P.; Ramesha, K.; Sathiya, M.; Tarascon, J.; Shukla, A. *Chem. Mater.* **2010,** 22, (9), 2857-2863.
17. Wolfenstine, J.; Allen, J. *J. Power Sources* **2008,** 180, (1), 582-585.
18. Shen, L.; Yuan, C.; Luo, H.; Zhang, X.; Xu, K.; Zhang, F. *J. Mater. Chem.* **2011,** 21, (3), 761-767.
19. Wang, D.; Choi, D.; Li, J.; Yang, Z.; Nie, Z.; Kou, R.; Hu, D.; Wang, C.; Saraf, L. V.; Zhang, J. *ACS nano* **2009,** 3, (4), 907-914.
20. Sun, Y.; Wu, Q.; Shi, G. *Energy Environ. Sci.* **2011,** 4, (4), 1113-1132.
21. Shi, Y.; Chou, S.-L.; Wang, J.-Z.; Wexler, D.; Li, H.-J.; Liu, H.-K.; Wu, Y. *J. Mater. Chem.* **2012,** 22, (32), 16465-16470.
22. Shi, Y.; Chou, S.; Wang, J.; Li, H.; Liu, H.; Wu, Y. *J. Power Sources* **2013,** 244, (0), 684-689.
23. Oh, S. W.; Myung, S. T.; Oh, S. M.; Oh, K. H.; Amine, K.; Scrosati, B.; Sun, Y. K. *Adv. Mater.* **2010,** 22, (43), 4842-4845.
24. Yang, J.; Wang, J.; Wang, D.; Li, X.; Geng, D.; Liang, G.; Gauthier, M.; Li, R.; Sun, X. *J. Power Sources* **2012,** 208, 340-344.
25. Wang, Y.; Feng, Z. S.; Chen, J. J.; Zhang, C. *Mater. Lett.* **2012,** 71, 54-56.
26. Tang, Y.; Huang, F.; Bi, H.; Liu, Z.; Wan, D. *J. Power Sources* **2012,** 203, 130-134.
27. Zhu, N.; Liu, W.; Xue, M.; Xie, Z.; Zhao, D.; Zhang, M.; Chen, J.; Cao, T. *Electrochim. Acta* **2010,** 55, (20), 5813-5818.
28. Tang, Y.; Huang, F.; Zhao, W.; Liu, Z.; Wan, D. *J. Mater. Chem.* **2012,** 22, (22), 11257-11260.
29. Murugan, A. V.; Muraliganth, T.; Manthiram, A. *J.Phys.Chem.C* **2008,** 112, (37), 14665-14671.
30. Murugan, A. V.; Muraliganth, T.; Manthiram, A. *J. Electrochem. Soc.* **2009,** 156, (2), A79-A83.
31. Chou, S. L.; Wang, J.; Liu, H.; Dou, S. X. *J.Phys.Chem.C* **2011,** 115, (32), 16220–16227.
32. Shi, Y.; Wen, L.; Li, F.; Cheng, H.-M. *J. Power Sources* **2011,** 196, (20), 8610-8617.
33. Zhang, Q.; Peng, W.; Wang, Z.; Li, X.; Xiong, X.; Guo, H.; Wang, Z.; Wu, F. *Ionics* **2013**, 1-7.